The Report Committee for You Wang
Certifies that this is the approved version of the following Report:

Estimating Capillary Pressure From NMR Measurements Using a Pore-Size-Dependent Fluid Substitution Method

APPROVED BY
SUPERVISING COMMITTEE:

Carlos Torres-Verdín, Supervisor

Zoya Heidari

Estimating Capillary Pressure From NMR Measurements Using a Pore-Size-Dependent Fluid Substitution Method

by

You Wang

Report

Presented to the Faculty of the Graduate School of

The University of Texas at Austin

in Partial Fulfillment

of the Requirements

for the Degree of

Master of Science in Engineering

The University of Texas at Austin

May 2019

Dedication

To my parents and grandparents for their love and support.

Acknowledgements

I would like to express my sincere gratitude to my supervisor, Dr. Carlos Torres-Verdín for his guidance and support. It is such an excellent experience to work in his group that I met many talented people. Profound gratitude goes to Dr. David Medillin for his guidance on the research and lab work. I am really indebted to him for helping me with every detail in my research. I also would like to thank Dr. Zoya Heidari for serving on my committee and Dr. Hugh Daigle for the access to the lab and NMR machine.

Thanks to Reynaldo Casanova for his administrative support. Additionally, I am appreciative to my peers in the research group. They are always willing to help and give suggestions. Special mention goes to Joshua Christopher Bautista-Anguiano for his support on experiments, and Mohammed Albusairi for his suggestions.

Finally, thanks go to my parents and grandparents for their unbelievable support.

Abstract

Estimating Capillary Pressure From NMR Measurements Using a Pore-Size-Dependent Fluid Substitution Method

You Wang, M.S.E

The University of Texas at Austin, 2019

Supervisor: Carlos Torres-Verdín

This report introduces a workflow to calculate capillary pressure curves from NMR transverse relaxation time (T_2) distributions of partially hydrocarbon-saturated measurements. First, a pore-size-dependent fluid-substitution (PSDFS) joint inversion method is developed to correct T_2 distributions for hydrocarbon effects in partially hydrocarbon-saturated rocks. A PSDFS joint inversion on the T_2 distributions of samples at different hydrocarbon saturations is used to estimate input parameters for fluid substitution and to reconstruct the fully water-saturated T_2 distribution. Next, the T_2 distribution of the fully water saturated sample is converted to a pore-size distribution using an estimated surface relaxivity. Finally, assuming a linear relationship between pore and throat size distributions, the saturation-dependent capillary pressure curve can be estimated using a triangular tube model.

The PSDFS joint inversion is validated on NMR measurements of Berea sandstone samples with different values of hydrocarbon saturation. The feasibility of our joint inversion method is confirmed by comparing the calculated fully water-saturated T_2

distribution to the T_2 distribution of the measured fully water-saturated rock sample. The capillary pressure curves are derived from fluid-substituted fully water-saturated T_2 distributions and compared to mercury injection capillary pressure (MICP) measurements. Capillary pressure curves derived with the PSDFS method agree well with MICP measurements.

Table of Contents

List of Tables

List of Figures

Chapter 1: Introduction

Capillary pressure vs saturation (Pc-Sat) curves are commonly measured in the laboratory through MICP, porous plate, or centrifuge methods. These methods, however, are expensive and time-consuming because they must be performed under restrictive laboratory conditions.

NMR-based methods have been proposed as alternative procedures to estimate Pc-Sat curves. There are, in general, two approaches for calculating Pc-Sat curves from NMR T_2 distributions: empirical approaches where the cumulative NMR porosity is calibrated to match the Pc-Sat curve, and physical approaches where physical models are used to convert the NMR T_2 distribution into a Pc-Sat curve.

In empirical approaches, the resemblance of the shape of the Pc-Sat curve and the cumulative T_2 distribution is used to calculate the Pc-Sat curve (Xiao and Zhang, 2008; Gao et al., 2011; Xiao, et al., 2016a; Xiao, et al., 2016b). Although these methods work well for rocks with uniform throat-size distributions, they lack physical support and can require substantial data to calibrate.

In physical approaches, the Pc-Sat curve is derived from the NMR T_2 distribution using petrophysical models. This is possible because both the Pc-Sat curve and the NMR T_2 distribution depend on the pore-space geometry; the former depends on the pore-throat-size distribution, while the latter on the pore-size distribution. Thus, in order to estimate Pc-Sat curves from NMR T_2 distributions, a relationship between pore-size and pore-throat must be used. Several relationships have been proposed but here the simplest, a linear relation, is chosen (Volokitin et al., 2001; Arogun and Nwosu, 2011; Raheem et al., 2017; Kadkhodaie et al., 2019).

In most cases, pore geometry is considered cylindrical or spherical. However, these geometries cannot account for pendular water present in partially saturated rocks. A triangular tube pore geometry has been introduced to improve the relationship between pore- and throat-size distributions for capillary pressure calculations (Grattoni et al., 2003; Mohnke et al., 2015; Hiller and Klitzsch, 2018).

NMR T_2 distributions can be used to calculate Pc-Sat curves only in single-fluid saturated rocks, for only then can they be interpreted as pore-size distributions and used to calculate Pc-Sat curves. When hydrocarbon is present, a correction to remove the hydrocarbon effect must be applied. Volokitin et al. (2001) and Altunbay et al. (2001) removed the hydrocarbon effect from T_2 distributions before using them for Pc-Sat curves derivations. However, Volokitin's method needs an empirical relationship between irreducible water saturation and the geometric mean of T_2 that must be calibrated with laboratory measurements.

Minh et al. (2016) extended Volokitin et al.'s (2001) method and combined it with factor analysis, where they decomposed the T_2 distributions into factors whose functional form are log-normal distributions. Unfortunately, not all T_2 distributions can be decomposed as a sum of log-normal distributions. Moreover, the major drawback of this method is that to calculate the fully water-saturated T_2 distribution, it requires the logarithmic T_2 mean of the fully water-saturated T_2 distribution, which we do not know *a-priori* and we are attempting to calculate, i.e., we must know *a-priori* something we can only know *a-posteriori.*

Medellin et al. (2019) proposed a pore-size-dependent fluid substitution method that does not require knowing any *a-posteriori* quantities *a-priori*. However, it requires exact knowledge of the contribution to the magnetization decay of the bulk hydrocarbon, which implies knowing *a-priori* the T_2 bulk value and total hydrocarbon pore volume.

In this report, the method presented in Medellin et al. (2019) is extended to develop a PSDFS joint inversion method so that we can prescind of the hydrocarbon parameters. Then, the fluid-substituted T_2 distribution at full water saturation is used to derive the Pc-Sat curve and compare it to those obtained from MICP measurements.

Chapter 2: Theory

2.1 PORE-SIZE-DEPENDENT FLUID SUBSTITUTION METHOD

We use the method developed by Medellin et al. (2019), which we briefly outline below.

Assuming a perfectly water-wet rock saturated with water and hydrocarbon, the first step consists of subtracting the bulk hydrocarbon contribution to the magnetization decay, $\mathbf{m}_{\mathrm{Bhc}}$, from the water-hydrocarbon magnetization decay, $\mathbf{m}_{\mathrm{whc}}$, and obtain the hydrocarbon-depleted magnetization decay, $\mathbf{m}_{\mathrm{hcd}}$, given by

$$\mathbf{m}_{\mathrm{hcd}} = \mathbf{m}_{\mathrm{whc}} - \mathbf{m}_{\mathrm{Bhc}}, \tag{2.1}$$

where $(\mathbf{m}_{\mathrm{whc}})_i = m_{\mathrm{whc}}(t_i)$. We assume that the bulk hydrocarbon contribution can be completely calculated, i.e., that we know the T_2 bulk value of hydrocarbon, as well as the fluid volume. Next, we calculate the T_2 distribution, $\mathbf{u}_{\mathrm{hcd}}$, of the hydrocarbon depleted magnetization decay by inverting

$$\mathbf{m}_{\mathrm{hcd}} = \mathbf{K}_{\mathrm{hcd}}\mathbf{u}_{\mathrm{hcd}}, \tag{2.2}$$

where $(\mathbf{K}_{\mathrm{hcd}})_{ij} = e^{-t_i/T_{2\mathrm{hcd},j}}$. Fluid substitution is achieved by transforming the T_2 value of each partially water-saturated pore to a larger T_2 value corresponding to a fully water-saturated pore using the transformation

$$\frac{1}{T_2^{(f)}} = \frac{S_{\mathrm{w}}^{*(i)}}{S_{\mathrm{w}}^{*(f)}}\frac{1}{T_2^{(i)}} + \left(1 - \frac{S_{\mathrm{w}}^{*(i)}}{S_{\mathrm{w}}^{*(f)}}\right)\frac{1}{T_{2\mathrm{Bw}}}, \tag{2.3}$$

where $T_2^{(f)}$ is the T_2 value at the final saturation state, $T_2^{(i)}$ is the T_2 value at the initial saturation state, $S_{\mathrm{w}}^{*(i)}$ and $S_{\mathrm{w}}^{*(f)}$ is the pore-size-dependent water saturation value at the initial and final states, respectively, and $T_{2\mathrm{Bw}}$ is the T_2 value of bulk water, which we set to 2511 ms. We use the step-function thin-film model as our pore-size-dependent water saturation distribution, which is defined as

$$S_{\mathrm{w}}^{*}=\begin{cases}1 & T_2 \le T_{2\mathrm{c}} \\ S_{\mathrm{w}}^{0} & T_2 > T_{2\mathrm{c}}\end{cases}, \tag{2.4}$$

and illustrated in Figure 2.1. All pores with radius $r < T_{2\mathrm{c}}\rho$ contain irreducible water and remain fully water-saturated, while pores with $r > T_{2\mathrm{c}}\rho$ contain thin water films. If we define the pore-size-dependent saturation matrix as

$$(\mathbf{S}_{\mathrm{w}}^{*})_{ij}=\mathrm{diag}\left(S_{\mathrm{w}}^{*}\left(T_{2j}\right)\right), \tag{2.5}$$

then the T_2 components of the water-saturated T_2 distribution, $\mathbf{u}_{\mathrm{ws}}$, are given by

$$\mathbf{u}_{\mathrm{ws}}=\left(\mathbf{S}_{\mathbf{w}}^{*}\right)^{-1}\mathbf{u}_{\mathrm{hcd}}\,. \tag{2.6}$$

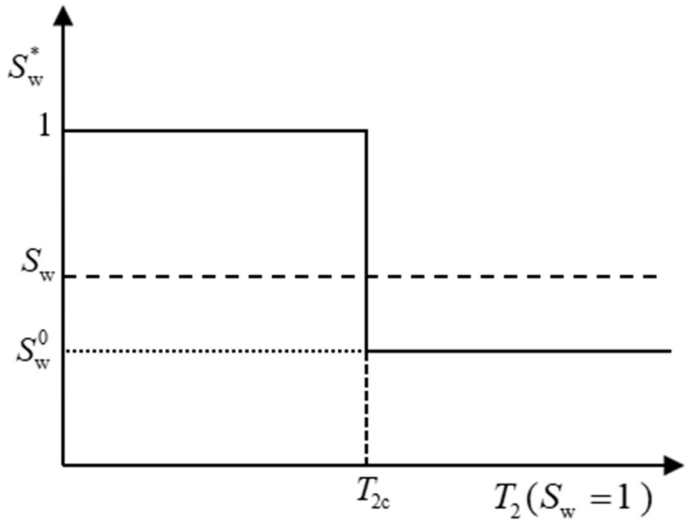

Figure 2.1: A step-function thin-film model. T_2 values of the x-axis correspond to T_2 values of the pores at full water saturation; S_{w}^{*} is the pore water-saturation as function of pore-size ($r = T_2\rho$); S_{w}^{0} is the individual pore water-saturation above the cut off value $T_{2\mathrm{c}}$; and S_{w} is the water saturation for all pores (Medellin et al., 2019).

2.2 CALCULATING THE PC-SAT CURVE

First, we assume $r_{\mathrm{pore}} = r_{\mathrm{throat}}$, and set the relaxivity of Berea sandstone to $\rho = 10\ \mu\mathrm{m/s}$. We use the Brownstein and Tarr equation,

$$\frac{1}{T_2} = \frac{1}{T_{2\mathrm{Bw}}} + \rho\frac{S}{V}, \tag{2.7}$$

to connect the T_2 distribution with the surface-to-volume ratio of the pore. Even though the step-function distribution can model thin films and is adequate for fluid substitution, it cannot capture the effect of pendular water, which is crucial to calculate Pc-Sat curves. Therefore, we use the triangular tube model to calculate the Pc-Sat curve. Assuming the pore to be a triangular equilateral tube, the surface-to-volume ratio is given by

$$\frac{S}{V} = \frac{4\sqrt{3}}{L}, \tag{2.8}$$

where L is the length of the sides of the equilateral triangular pore. A triangular pore will undergo drainage when the capillary pressure causes the pendular water to reach a critical radius of curvature, r_c, given by (Monhnke et al., 2015)

$$r_\mathrm{c} = P\left(\frac{1}{2G} + \sqrt{\frac{\pi}{G}}\right)^{-1} = 3L_\mathrm{c}\left(\frac{1}{2G} + \sqrt{\frac{\pi}{G}}\right)^{-1}, \tag{2.9}$$

with

$$G = \frac{A}{P^2} = \frac{\sqrt{3}}{36}, \tag{2.10}$$

A being the cross-section area of the triangle, and P the perimeter. The corresponding capillary pressure is therefore written as

$$P_\mathrm{c} = \sigma\cos\theta\left(\frac{1}{R_1} + \frac{1}{R_2}\right) = \frac{\sigma\cos\theta}{r_\mathrm{c}}, \tag{2.11}$$

where $R_1 = r_\mathrm{c}$, and $R_2 = \infty$. The water saturation at this pressure is given by

$$S_\mathrm{w} = \frac{\sum\limits_{L_i<L_\mathrm{c}} L_i^2 + \frac{4}{\sqrt{3}}\sum\limits_{L_i>L_\mathrm{c}} (3\sqrt{3}r_\mathrm{c}^2 - \pi r_\mathrm{c}^2)}{\sum\limits_{L_i} L_i^2}, \tag{2.12}$$

2.3 FLUID SUBSTITUTION JOINT INVERSION METHOD

The major drawback of Medellin et al.'s (2019) method is that the precise amount of hydrocarbon and its T_2 bulk value must be known a-priori. In practice, it is not always possible to estimate individual hydrocarbon T_2 values nor the total hydrocarbon volume, e.g., when the hydrocarbon and water T_2 peaks overlap. To overcome these difficulties, we propose a pore-size-dependent fluid-substitution (PSDFS) joint inversion method to perform the hydrocarbon correction. The PSDFS joint inversion method needs at least two NMR decay signals at different saturations as input measurements. The joint-inversion is carried out by enforcing consistency between the fluid-substituted NMR T_2 distributions that result from each partially water-saturated data set. This is achieved by solving simultaneously a set of 12 relations in the least-squares sense, i.e., by minimizing a cost function dependent on 12 terms (C_1 through C_{12}) – equal to the number of unknown parameters.

The terms are:

1) C_1 and C_2, terms relating the pore water-saturation to the T_2 cut off in each sample:

$$C_1 = S^0_{\mathrm{w},1} - \frac{T_{2\mathrm{l},1}(T_{2\mathrm{Bw}} - T_{2\mathrm{c}})}{T_{2\mathrm{c}}(T_{2\mathrm{Bw}} - T_{2\mathrm{l},1})}, \tag{2.13}$$

$$C_2 = S^0_{\mathrm{w},2} - \frac{T_{2\mathrm{l},2}(T_{2\mathrm{Bw}} - T_{2\mathrm{c}})}{T_{2\mathrm{c}}(T_{2\mathrm{Bw}} - T_{2\mathrm{l},2})}, \tag{2.14}$$

where $T_{2\mathrm{c}}$ is the T_2 cut off value used in the step-function pore-size-dependent water saturation profile, $S^0_{\mathrm{w},1(2)}$ are the water saturation values for $T_2 > T_{2\mathrm{c}}$, $T_{2\mathrm{l},1(2)}$ are the T_2 cut off values under which all water is bound water [see Medellin et al, 2019, Eq. (24)], and $T_{2\mathrm{Bw}}$ is the T_2 value of bulk water. The subscripts 1 and 2 refer to the sample with partial water saturation 1 and 2, respectively.

2) C_3-C_4, terms relating the total porosity of the sample derived from the pore-size-dependent saturation profile and the overall sample saturation at a given saturation state:

$$C_3 = \sum_k \left(\mathbf{H}_{\text{hcd},1}^{-1}\mathbf{u}_{\text{hcd},1}\right)_k - \left(\mathcal{H}_{\text{hcd},1}\right)^{-1}\sum_k \left(\mathbf{u}_{\text{hcd},1}\right)_k , \tag{2.15}$$

$$C_4 = \sum_k \left(\mathbf{H}_{\text{hcd},2}^{-1}\mathbf{u}_{\text{hcd},2}\right)_k - \left(\mathcal{H}_{\text{hcd},2}\right)^{-1}\sum_k \left(\mathbf{u}_{\text{hcd},2}\right)_k , \tag{2.16}$$

where $\mathbf{H}_{\text{hcd}}$ is the pore-size-dependent hydrogen index of the hydrocarbon depleted signal, and $\mathcal{H}_{\text{hcd}}$ is the overall hydrogen index of the hydrocarbon-depleted signal. They are given by

$$\mathbf{H}_{\text{hcd}} = \mathbf{S}_{\text{w}}^{*}\mathcal{H}_{\text{w}}, \tag{2.17}$$

$$\mathcal{H}_{\text{hcd}} = S_{\text{w}}\mathcal{H}_{\text{w}} , \tag{2.18}$$

where $\mathcal{H}_{\text{w}}$ is the hydrogen index of water, and S_{w} is the overall water saturation.

3) C_5-C_6, terms equating the pore volume below and above the T_2 cut off value T_{2c}:

$$C_5 = \sum_k^{T_{2k}<T_{2c}} \left(\mathbf{u}_{\text{hcd},1}\right)_k - \sum_k^{T_{2k}<T_{2c}} \left(\mathbf{u}_{\text{hcd},2}\right)_k , \tag{2.19}$$

$$C_6 = \sum_{T_{2k}>T_{2c}} \left(\mathbf{H}_{\text{hcd},1}^{-1}\mathbf{u}_{\text{hcd},1}\right)_k - \sum_{T_{2k}>T_{2c}} \left(\mathbf{H}_{\text{hcd},2}^{-1}\mathbf{u}_{\text{hcd},2}\right)_k , \tag{2.20}$$

where the sum in C_5 is over all k's such that $T_{2k} < T_{2c}$, and the sum in C_6 is over all k's such that $T_{2k} > T_{2c}$.

4) C_7 and C_8, terms relating the total porosity of the sample in the same saturation state at different fluid substitution stages

$$C_7 = \mathcal{H}_{\text{whc},1}^{-1}\sum_k \left(\mathbf{u}_{\text{whc},1}\right)_k - \mathcal{H}_{\text{hcd}}^{-1}\sum_k \left(\mathbf{u}_{\text{hcd},1}\right)_k , \tag{2.21}$$

$$C_8 = \mathcal{H}_{\text{whc},2}^{-1}\sum_k \left(\mathbf{u}_{\text{whc},2}\right)_k - \mathcal{H}_{\text{hcd},2}^{-1}\sum_k \left(\mathbf{u}_{\text{hcd},2}\right)_k , \tag{2.22}$$

where $\mathcal{H}_{\text{whc}}$ is the overall hydrogen index of the water-hydrocarbon-saturated signal, given by

$$\mathcal{H}_{\text{whc}} = S_{\text{w}}\mathcal{H}_{\text{w}} + (1-S_{\text{w}})\mathcal{H}_{\text{hc}}, \tag{2.23}$$

with $\mathcal{H}_{\text{hc}}$ being the hydrogen of the hydrocarbon.

5) C_9, a term relating the total porosity of the sample derived from two different saturation states

$$C_9 = \mathcal{H}_{\text{whc},1}^{-1}\sum_k \left(\mathbf{u}_{\text{whc},1}\right)_k - \mathcal{H}_{\text{whc},2}^{-1}\sum_k \left(\mathbf{u}_{\text{whc},2}\right)_k, \tag{2.24}$$

6) C_{10}, a term equating the forward models of the fluid substituted distributions from both saturation states

$$C_{10} = \mathbf{K}_{\text{ws},1}\mathbf{u}_{\text{ws},1} - \mathbf{K}_{\text{ws},2}\mathbf{u}_{\text{ws},2}, \tag{2.25}$$

7) C_{11} and C_{12}, two terms enforcing consistency between the intermediate stages of fluid substitution

$$C_{11} = \mathbf{K}_{\text{whc},2}\mathbf{u}'_{\text{whc},2} - \mathbf{K}_{\text{whc},2}\mathbf{u}_{\text{whc},2}, \tag{2.26}$$

$$C_{12} = \mathbf{K}_{\text{whc},1}\mathbf{u}'_{\text{whc},1} - \mathbf{K}_{\text{whc},1}\mathbf{u}_{\text{whc},1}, \tag{2.27}$$

where $\mathbf{u}'_{\text{whc},1(2)}$ is the water-hydrocarbon T_2 distribution obtained from the hydrocarbon-depleted T_2 distribution of the other saturation state, $\mathbf{u}_{\text{hcd},2(1)}$.

These twelve relations are used to find the best fluid substitution parameters: $\{S^0_{\text{w},1}, S^0_{\text{w},2}, T_{2\text{c}}, \text{H}_{\text{w}}, \text{H}_{\text{hc}}, S_{\text{w},1}, S_{\text{w},2}, T_{2\text{l},1}, T_{2\text{l},2}, T_{2\text{Bhc},1}, T_{2\text{Bhc},2}, f_{\text{hc}1}\}$. Here, $T_{2\text{Bhc},1(2)}$ are the T_2 bulk components of the bulk hydrocarbon, and $f_{\text{hc}1}$ is the volume fraction contribution to the total hydrocarbon pore volume of the first hydrocarbon component (assuming the T_2 distribution of the hydrocarbon is doubly peaked).

2.4 WORKFLOW

The workflow is illustrated in Figure 2.2 and consists of two steps. First, fluid substitution is applied to a set of T_2 distributions from a sample at different water saturations (or from similar samples). Self-consistent relations (Eqs. (2.13)-(2.27)) are enforced to obtain the best fluid substitution parameters. Second, we derive a Pc-Sat curve by assuming fast-diffusion, a realistic value for pore relaxivity, and a triangular pore model.

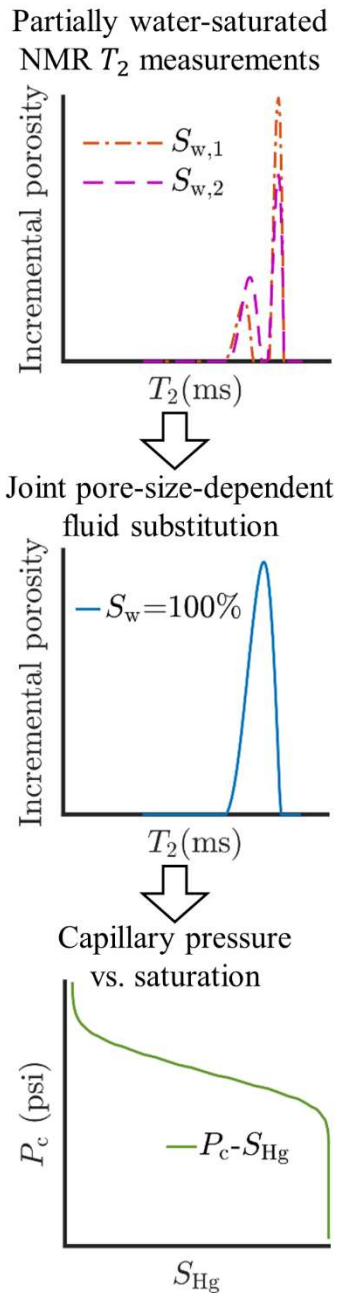

Figure 2.2 Workflow for calculating the capillary pressure vs saturation curve using a joint-inversion pore-size-dependent fluid-substitution method. (Top) fluid substitution is applied to two partially water-saturated T_2 distributions to obtain (middle) a water-saturated T_2 distribution, which is then converted to (bottom) a Pc-Sat curve.

Chapter 3: Methods

3.1 EXPERIMENT

3.1.1 Sample Preparation

PSDFS joint inversion is applied to the measurements of two Berea sandstone samples, E7 and E9. The Berea samples are oven-dried first. They are then vacuum-saturated with 5% wt NaCl brine. We use a centrifuge to desaturate the samples to different water saturation levels. The water saturation of Berea E7 and Berea E9 is 0.385 and 0.843, respectively. Next, the samples are put back in the vacuum to saturate them with olive oil. Refer to Table 1 for detailed information on the Berea sandstone samples.

	Berea E7	Berea E9
Diameter (mm)	37.9	37.9
Length (mm)	36.9	36.9
Porosity	0.205	0.207
$\boldsymbol{S_w}$	0.385	0.843

Table 1: Description of the Berea sandstone samples.

3.1.2 MICP Measurements

Two Berea sandstone samples are cut into 25 mm by 25 mm cylinders. The porosities of the samples are 0.205 and 0.207, respectively. We set the surface tension of mercury at 485 dynes/cm and the advance and receding contact angle at 130 degrees.

3.1.3 NMR Parameters and Measurements

All measurements were acquired with an Oxford Geospec2 NMR spectrometer working at 2.17 MHz using a Carr-Purcell-Meiboom-Gill (CPMG) pulse sequence. The signal to noise ratio for all measurements is above 200. Refer to Table 2 for experimental parameters. The T_2 magnetization decay measurements of the fully water-saturated E7 and E9 samples are acquired before the centrifuge. The T_2 magnetization decays of the water-hydrocarbon-saturated samples E7 and E9 are obtained after re-saturating with olive oil.

	Water-hydrocarbon saturated samples		Water-saturated samples	
	Berea E7	Berea E9	Berea E7	Berea E9
S_{w}	0.385	0.843	1	1
Echo number	14925	18657	29851	29851
Waiting time (s)	3	3.75	6	6
Inter-echo time (ms)	0.134	0.134	0.134	0.134
Scans	48	16	32	32

Table 2. Experimental NMR parameters.

3.2 INVERSION

The T_2 distributions are obtained through a nonnegative least-squares minimization algorithm (Lawson-Dawson) using 121 logarithmically spaced points between $T_2 = 10^{-2}$ ms and $T_2 = 10^4$ ms. The regularization parameter of the measurement of Berea E7 at S_w=38% was chosen using the discrepancy principle, yielding a value of 3.2. Given that the signal-to-noise ratio of the other measurements was comparable, the regularization parameter for the remaining measurements was then fixed at 3.2.

For the joint inversion, we use two NMR magnetization decays of two rock samples at different values of water saturation. The porosities of the two samples differ by 1% and can be considered equal. If the porosities of the two rock samples were very different, a porosity correction would be needed before the joint inversion. We use bounded least squares to minimize the sum of the squares of all the C-terms.

Chapter 4: Results

We apply our PSDFS joint inversion method to two NMR data sets, one from a sample at S_w =38% and a second one at S_w =84%, and obtain two fluid-substituted NMR T_2 distributions at S_w=100%. Figure 4.1 shows the magnetization decay of the fully water-saturated sample (Data S_w=100%), the partially water-saturated samples (Data S_w=38% and Data S_w=84%), as well as the resulting fluid-substituted (PSDFS from S_w=38% and PSDFS from S_w=84%) magnetization decays derived from the partially water-hydrocarbon-saturated data sets. Figure 4.2 shows the corresponding T_2 distributions of the magnetization decays described in Figure 4.1.

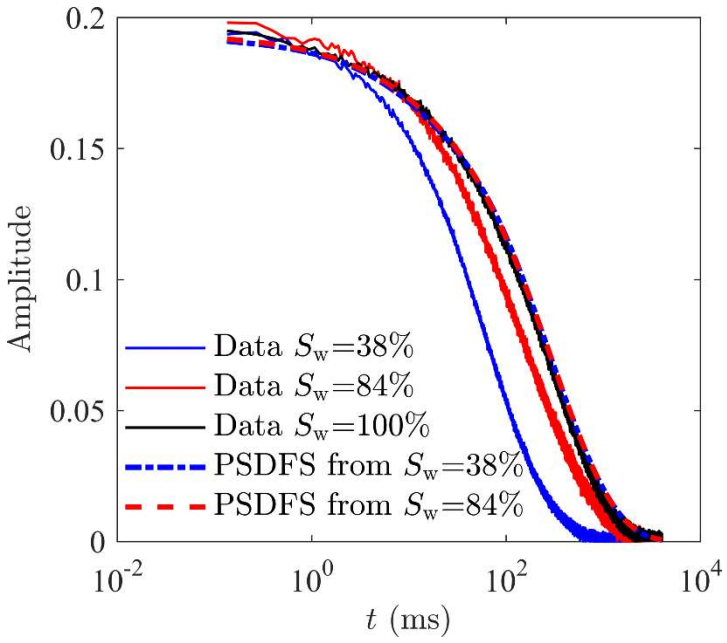

Figure 4.1 Magnetization T_2 decay of: (solid blue) the sample at S_w=38%, and (solid red) the sample at S_w=84%, (solid black) a fully water-saturated sample, (dash blue) the fluid-substituted T_2 distribution from S_w=38%, and (dash red) the fluid-substituted T_2 distribution from S_w=84%.

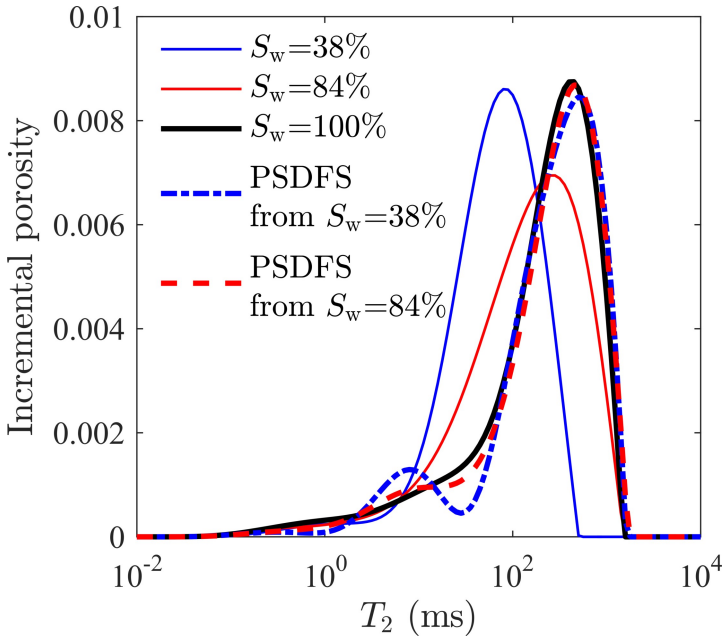

Figure 4.2 T_2 distributions of: (solid blue) the sample at S_w=38%, (solid red) the sample at S_w=84% (solid red), (dashed blue) the fluid-substituted T_2 distribution from S_w=38%, and (dashed red) the fluid-substituted T_2 distribution from S_w=84%.

Next, we use a triangular tube pore model and Eqs. (2.7)-(2.12) to obtain Pc-Sat curves from fluid-substituted T_2 distributions. The derived Pc-Sat curves (PSDFS from S_w=38% and PSDFS from S_w=84%) are compared to the ones derived from MICP measurements (MICP) in Figure 4.3. The Pc-Sat curves derived directly from the partially water-saturated and fully water-saturated NMR data sets are also shown in Figure 4.3 for comparison.

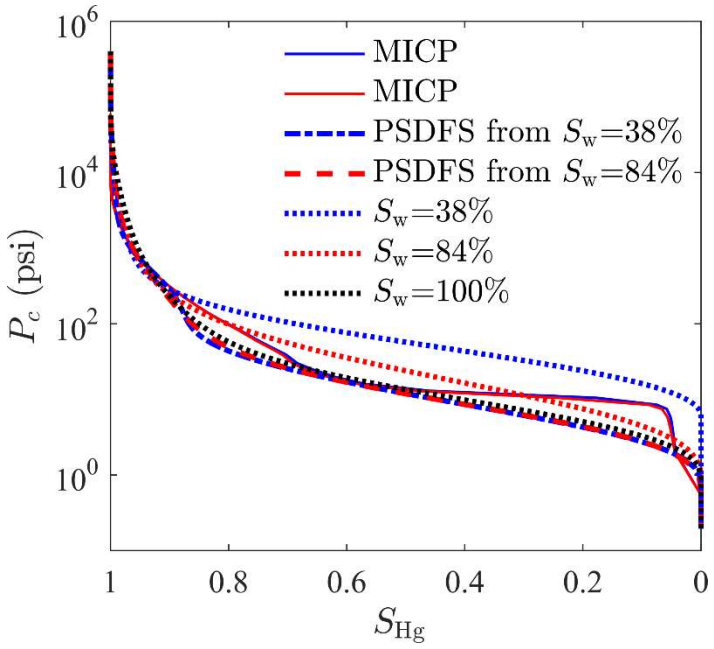

Figure 4.3 Pc-Sat curves derived from: (solid blue and solid red) two MICP measurements, (dash blue and dash red) fluid-substituted T_2 distributions obtained through PSDFS joint inversion, (dotted blue and dotted red) the original partially water-saturated T_2 distributions, and (dotted black) the fully water-saturated T_2 distribution.

Chapter 5: Disscussion and Conclusions

5.1 DISSCUSSION

For the PSDFS joint inversion we used a spherical pore model, while the Pc-Sat curve calculation we used a triangular pore model. There are several reasons why we used two different pore models.

Whereas a triangular pore can readily model pendular water and the effect that capillary pressure has on water saturation, a spherical pore can only model thin films of water and cannot capture the effect of capillary pressure on residual water saturation. This condition makes the triangular pore more suitable for calculating Pc-Sat curves.

However, because the surface-to-volume ratio of all partially water-saturated triangular pores is the same, they have the same T_2 value and thus are not amenable for fluid substitution. A spherical pore model with a step-function saturation profile, on the other hand, can capture the T_2 dependence on pore size. This makes the spherical pore with a step-function saturation profile more suitable for our PSDFS method.

The spherical pore with a step-function water saturation profile does introduce an adverse effect in our PSDFS method, as can be observed in Figure 4.2, where the PSDFS T_2 distributions from both samples exhibit an oscillation at approximately $T_2 = 10$ ms, the one corresponding to the sample at S_{w}=38% being larger. This oscillation is a consequence of the degeneracy of T_2 values between small fully water-saturated pores and large partially water-saturated pores with thin water films. In our PSDFS method, we assume all porosity with $T_2 < T_{2\mathrm{c}}$ belongs completely to small water-saturated pores. This approximation is valid at high water saturation, but starts to break down at lower values of water saturation, which explains why samples with higher water saturation produce better fluid-substituted T_2 distributions (see Figure 4.2). Consequently, after

performing the PSDFS joint inversion method, we use the NMR data set of the sample with highest water-saturation level to calculate the fully water-saturated T_2 distribution.

Figure 4.3 shows the Pc-Sat curves measured with MICP as well as those derived from NMR T_2 distributions. We observe that the Pc-Sat curves derived from the fluid-substituted T_2 distributions (PSDFS) not only match the Pc-Sat curve derived from the fully water-saturated T_2 distribution (S_w=100%), but they also yield a better match to the MICP curve than the Pc-Sat curves derived from the uncorrected partially water-saturated T_2 distributions (S_w=38% and S_w=84%).

The workflow above is limited to water-wet rocks with negligible internal field gradients for which a correlation between pore and throat size exists. Consequently, it is not well suited for complex pore networks with mixed wettability. Additionally, a low signal to noise ratio together with uncertainty in pore and throat size determination due to NMR tool ringing and echo time limitations can impact the determination of Pc-Sat curves.

5.2 CONCLUSIONS

The NMR pore-size-dependent joint fluid substitution method developed in this report enables the calculation of capillary pressure vs saturation (Pc-Sat) curves from partially water-saturated T_2 distributions.

Using a combination of spherical and triangular pore models, we verified that the NMR fluid-substituted-derived Pc-Sat curves show an improved match with MICP measurements over the Pc-Sat curves derived from the partially water-saturated T_2 distributions. Moreover, we showed that the necessary input parameters for fluid substitution can be directly estimated from NMR measurements using a joint-inversion pore-size-dependent fluid substitution method.

Acronyms

Bhc	bulk hydrocarbon
Bw	bulk water
CPMG	Carr-Purcell-Meiboom-Gill
HCD, hcd	hydrocarbon depleted
HC, hc	hydrocarbon
MICP	mercury injection capillary pressure
NMR	nuclear magnetic resonance
PSDFS	pore-size-dependent fluid substitution
Pc-Sat	Capillary pressure vs. saturation
W, w	water
WHC, whc	water hydrocarbon
WS, ws	water-saturated

Symbols

A	cross-section area of a pore
C	cost function
f_{hc1}	volume fraction contribution to the total hydrocarbon volume of the first hydrocarbon component
G	pore shape dependent parameter
H	pore-size dependent hydrogen index
$\mathcal{H}$	overall hydrogen index
(i), (f)	initial state, final state
K	T_2 kernel
L	side length of the equilateral triangular pore
L_{c}	critical side length of the equilateral triangular pore
m	T_2 magnetization decay
P	perimeter of the cross-section
P_{c}	capillary pressure
r	pore radius
r_{c}	critical radius of curvature
$R_{1,2}$	principal radii of curvature of the meniscus
S_{w}	water saturation
S_{w}^{*} , $\mathrm{S}_{\mathrm{w}}^{*}$	pore-size-dependent water-saturation distribution scalar, matrix
S_{w}^{0}	water-saturation level of partially saturated pores
$\frac{S}{V}$	surface to volume ratio of a pore
T_2	transverse relaxation time

T_{2c}	T_2 cut off value
T_{2l}	T_2 value under which all water is bound water
t	time
u	T_2 incremental porosity
$u'_{whc,1(2)}$	water-hydrocarbon T_2 incremental porosity obtained from the hydrocarbon depleted T_2 incremental porosity of the other saturation state, $u_{hcd,2(1)}$
ρ	surface relaxivity
θ	contact angle
σ	interfacial tension

References

Altunbay, M., Martain, R., and Robinson, M., 2001, Capillary Pressure Data From NMR Logs and its Implications on Field Economics, SPE Annual Technical Conference and Exhibition, New Orleans, Louisiana, USA, 30 September–3 October, doi:10.2118/71703-MS.

Arogun, O., and Nwosu, C., 2011, Capillary Pressure Curves from Nuclear Magnetic Resonance log Data in a Deepwater Turbidite Nigeria Field - A Comparison to Saturation Models From SCAL Drainage Capillary Pressure Curves, Nigeria Annual International Conference and Exhibition, Abuja, Nigeria, 30 July–3 August, doi:10.2118/150749-MS.

Gao, B., Wu, J., Chen, S., Kwak, H., and Funk, J., 2011, New Method for Predicting Capillary Pressure Curves from NMR Data in Carbonate Rocks, SPWLA 52nd Annual Logging Symposium, Colorado Springs, Colorado, USA, 14–18 May.

Grattoni, C.A., Al-Mahrooqi, S.H., Moss, A.K., Muggeridge, A.H., and Jing, X.D., 2003, An Improved Technique for Deriving Drainage Capillary Pressure from NMR T2 Distributions, International Symposium of the Society of Core Analysts, Pau, France, 21–24.

Hiller, T., and Klitzsch, N., 2018, Joint Inversion of Nuclear Magnetic Resonance Data From Partially Saturated Rocks Using a Triangular Pore Model, Geophysics, Vol. 83, no. 4, p. JM15–JM28, doi:10.1190/geo2017-0697.1.

Kadkhodaie, A., Rezaee, R., and Kadkhodaie, R., 2019, An Effective Approach to Generate Drainage Representative Capillary Pressure and Relative Permeability Curves in the Framework of Reservoir Electrofacies, Journal of Petroleum Science and Engineering, Vol. 176, p. 1082–1094, doi:10.1016/j.petrol.2019.01.098.

Medellin, D., Ravi, V.R., and Torres-Verdín, C., 2019, Pore-Size-Dependent Fluid Substitution Method for Magnetic Resonance Measurements, Geophysics, Vol. 84, no. 1, p. D25–D38, doi:10.1190/geo2017-0457.1.

Minh, C.C., Jain, V., Griffiths, R., and Maggs, D., 2016, NMR T2 Fluids Substitution, SPWLA 57th Annual Logging Symposium, Reykjavik, Iceland, 25–29 June.

Mohnke, O., Jorand, R., Nordlund, C., and Klitzsch, N., 2015, Understanding NMR Relaxometry of Partially Water-Saturated Rocks, Hydrology and Earth System Sciences, Vol. 19, no. 6, p. 2763–2773, doi:10.5194/hess-19-2763-2015.

Raheem, O.N., Fernandes, M.O., Thomas, N.C., Hashem, M.H., and Sulemana, N.T., 2017, Using NMR T2 to Predict the Drainage Capillary Curves Pc-Sw in Carbonates Reservoirs, SPE Reservoir Characterisation and Simulation Conference and Exhibition, Abu Dhabi, UAE, 8–10 May, doi:10.2118/185989-MS.

Volokitin, Y., Looyestijn, W.J., Slijkerman, W.F., and Hofmanl, J.P., 2001, A Practical Approach to Obtain Primary Drainage Capillary Pressure Curves From NMR Core and log Data, Petrophysics,Vol. 42, no. 4, p. 10.

Xiao, L., Mao, Z., Zou, C., Jin, Y., and Zhu, J., 2016a, A new Methodology of Constructing Pseudo Capillary Pressure (Pc) Curves From Nuclear Magnetic Resonance (NMR) Logs, Journal of Petroleum Science and Engineering, Vol. 147, p. 154–167, doi:10.1016/j.petrol.2016.05.015.

Xiao, L., Zou, C., Mao, Z., Jin, Y., and Zhu, J., 2016b, A new Technique for Synthetizing Capillary Pressure (Pc) Curves Using NMR Logs in Tight gas Sandstone Reservoirs, Journal of Petroleum Science and Engineering, Vol. 145, p. 493–501, doi:10.1016/j.petrol.2016.06.002.

Xiao, L., and Zhang, W., 2008, A New Method to Construct Reservoir Capillary Pressure Curves Using NMR log Data and its Application, Applied Geophysics, Vol. 5, no. 2, p. 92–98, doi:10.1007/s11770-008-0017-3.